EUROPEAN ORGANIZATION FOR NUCLEAR RESEARCH

Proposal to the ISOLDE and Neutron Time-of-Flight Committee

Unraveling the local structure of topological crystalline insulators using hyperfine interactions

January 11, 2016

L.M.C. Pereira[1], G. Springholz[2], J. Schell[3,4], J.G. Correia[5], H.P. Gunnlaugsson[1,3], T.E. Molholt[3], S. Cottenier[6], M. Deicher[4], V. Augustyns[1], T.A.L. Lima[1], G. Lippertz[1], J. McNulty[1], A. Fenta[1,7]

[1] *KU Leuven, Instituut voor Kern- en Stralingsfysica, 3001 Leuven, Belgium*
[2] *Institut für Halbleiter und Festkörperphysik, Johannes Kepler Universität, 4040 Linz, Austria*
[3] *CERN, PH Div, CH-1211 Geneve 23, Switzerland.*
[4] *Technische Physik, Universität des Saarlandes, 66041 Saarbrücken, Germany*
[5] *Centro de Ciências e Tecnologias Nucleares, Instituto Superior Técnico, Universidade de Lisboa, 2686-953, Sacavém, Portugal*
[6] *Center for Molecular Modeling, Ghent University, 9000 Gent, Belgium*
[7] *University of Aveiro, 3810-193 Aveiro, Portugal*

Spokesperson: L.M.C. Pereira [lino.pereira@fys.kuleuven.be]
Contact person: J. Schell [juliana.schell@cern.ch], J.G. Correia [Guilherme.Correia@cern.ch]

CERN-INTC-2016-005 / INTC-P-455
11/01/2016

Abstract:

Phenomena emerging from relativistic electrons in solids have become one the main topical subjects in condensed matter physics. Among a wealth of intriguing new phenomena, several classes of materials have emerged including graphene, topological insulators and Dirac semimetals. This project is devoted to one such class of materials, in which a subtle distortion of the crystalline lattice drives a material through different topological phases: Z_2 topological insulator (Z_2-TI), topological crystalline insulator (TCI), or ferroelectric Rashba semiconductor (FERS). We propose to investigate the local structure of $Pb_{1-x}Sn_xTe$ and $Ge_{1-x}Sn_xTe$ (with x from 0 to 1) using a combination of experimental techniques based on hyperfine interactions: emission Mössbauer spectroscopy (eMS) and perturbed angular correlation spectroscopy (PAC). In particular, we propose to study the effect of composition (x in $Pb_{1-x}Sn_xTe$ and $Ge_{1-x}Sn_xTe$) on (1) the magnitude of the rhombohedral distortion, and on (2) the

nature of the cubic-to-rhombohedral phase transition at temperature T_C (i.e. if displacive or order-disorder). The combination of these studies with those on the topology (by means of angle-resolved photoemission spectroscopy) will allow us to draw the topological phase diagram of $Pb_{1-x}Sn_xTe$ and $Ge_{1-x}Sn_xTe$, i.e. how the topological phase (Z_2-TI, TCI, FERS, or trivial) is determined by the rhombohedral distortion.

Requested shifts: [15] shifts, (split into [8] runs over [2] years)

1 Introduction

Topological crystalline insulators (TCI) are a new class of materials that fundamentally differ from conventional Z_2 topological insulators (Z_2-TI) such as Bi_2Se_3 in the sense that the topological character of the topological surface states (TSS) originates from the crystal mirror symmetry with respect to the (110) planes (rather than from time reversal symmetry as in Z_2-TI). The existence of gapless TSS was indeed theoretically predicted in the narrow gap semiconductor SnTe and its solid solutions with PbTe (i.e. $Pb_{1-x}Sn_xTe$).[2] TCI materials provide many means of tuning the topological properties by varying temperature, composition and lattice structure. In particular, a topological-to-trivial transition has been predicted when breaking the mirror symmetry e.g., by strains, magnetic dopants,[3] electric fields[4] or by hybridizing of the TSS in ultrathin film geometries.[5] Soon after theoretical prediction, the existence of a TSS was experimentally verified for (001) and (111) oriented SnTe[6;7] and $Pb_{1-x}Sn_xTe$.[8]
In a closely related class of materials, with the particularity of exhibiting broken inversion symmetry, spin-orbit coupling induces a Rashba spin splitting of electron states, manifested by a k-dependent splitting of the bands. Up to now, most research has focused on surface states and 2D electron gasses, but recently, a three-dimensional (3D) form of such Rashba-effect was discovered in the bismuth tellurohalides BiTeX (X=I, Br, or Cl).[9–11] In spite of the very large spin-splitting in these materials, they lack the possibility to switch or tune the spin texture. As proposed by recent work, this limitation can be overcome in a new class of functional materials displaying Rashba-splitting induced by a rhombohedral distortion of an otherwise cubic (*rocksalt*) structure [Fig. 1 (a)]: the so-called ferroelectric Rashba semiconductors (FERS).[12;13] GeTe is the most prominent example of such a material, since it undergoes a paraelectric (cubic) to ferroelectric (rhombohedral) phase transition [Fig. 1 (a)] at a Curie temperature (T_C) of ~ 670 K. In these materials, ferroelectricity was predicted to result in fully spin-polarized electronic bands with a spin

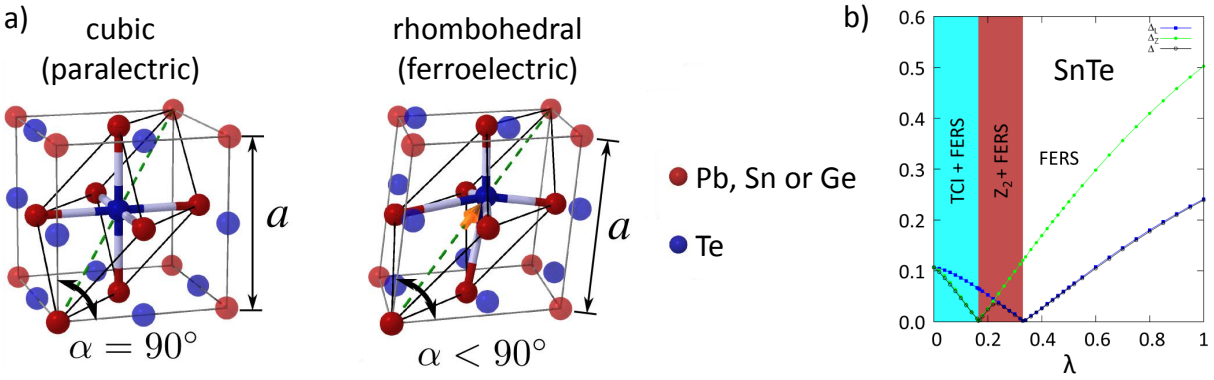

Figure 1: (a) Lattice structure of $Pb_{1-x}Sn_xTe$ and $Ge_{1-x}Sn_xTe$ in the cubic (paraelectric) phase and in the rhombohedrally distorted (ferroelectric) phase. The orange arrow indicates the sublattice displacement (relative displacement between Pb/Sn/Ge and Te sublattices). (b) Proposed topological phase diagram of SnTe as a function of the sublattice displacement parameter λ ($\lambda = 0$ in the cubic phase and $\lambda = 1$ in the rhombohedral phase).[1]

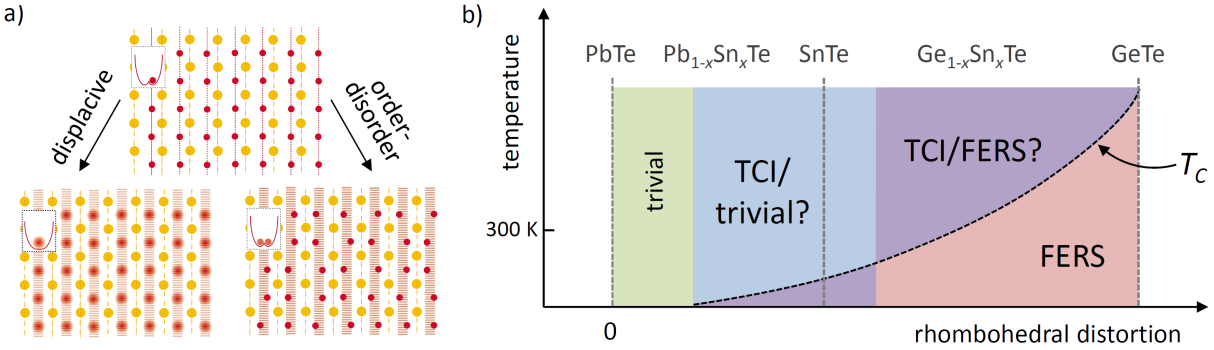

Figure 2: (a) Schematic illustration of a displacive (left) and order-disorder (right) transitions starting from the rhombohedrally distorted phase. (b) Simplified representation of the expected topological phase diagram of $Pb_{1-x}Sn_xTe$ and $Ge_{1-x}Sn_xTe$ in which an increase in x is linked to an increase in rhombohedral distortion, which in turn determines the topological state. The role of temperature is associated with the structural (cubic-to-rhombohedral) phase transition at T_C. For simplicity, the diagram does not explicitly include the direct effect of composition on the band structure (band inversion) and consequently on the topological state.

chirality directly coupled to the ferroelectric polarization even for the topologically trivial state.[12;13]

Cubic-to-Rhombohedral distortion. The rhombohedral distortion is one of the key parameters determining the topological phase (trivial, TCI, FERS, or even Z_2-TI) in these compounds [Fig. 1 (a)]. For example, in SnTe, a complex topological phase diagram has been predicted as a function of the size of the rhombohedral distortion [Fig. 1 (b)], including regions of coexistence of different non-trivial topological states.[1] The cubic-to-rhombohedral distortion consists of the elongation along the cube diagonal (111) accompanied by a sublattice displacement (relative displacement between Pb/Sn/Ge and Te sublattices), and can therefore be described by two key parameters: the angle α between $\vec{a}$ and $\vec{c}$ (90° in the cubic phase); the sublattice displacement Δr of the atom which would otherwise be in the geometric center of the rhombohedral cell (orange arrow in Fig. [Fig. 1 (b)]). The magnitude of the distortion and the associated T_C can be tuned by the composition x in $Pb_{1-x}Sn_xTe$ and $Ge_{1-x}Sn_xTe$ between the binary cases: GeTe with $\Delta r \approx 0.25$ Å and $T_C \approx 670$ K; SnTe with $\Delta r \approx 0.07$ Å and $T_C \approx 100$ K; PbTe, which is not distorted ($\alpha = 0$) but has recently been reported to develop a Δr from 0 Å at 15 K up to ~ 0.2 Å at 500 K.[14]

In order to draw the topological phase diagram, it is not only crucial to know the magnitude of the distortion below T_C (i.e. the deviation from $\alpha = 90°$ and $\Delta r = 0$ in the rhombohedral phase), but also above T_C. Interestingly, it has recently been argued[15;16] that the transition in GeTe and SnTe is not of a *displacive* nature as had been believed but arises from an *order-disorder* transition with local distortions preserved across the transition temperature (Fig. 2): although the lattice becomes cubic ($\alpha \approx 90°$) above T_C, the sublattice displacement ($\Delta r \neq 0$) is locally preserved (though randomly, i.e. not in an

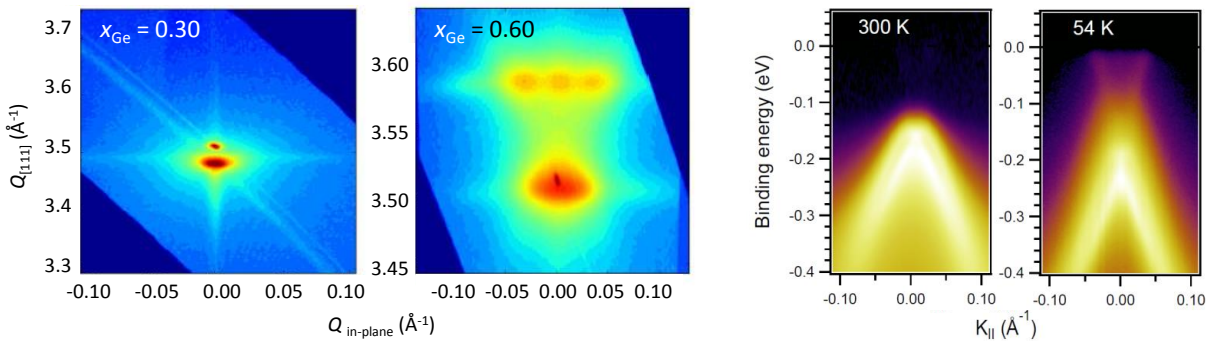

Figure 3: (*left*) Room temperature X-ray diffraction reciprocal space maps of the (222) Bragg reflection of $Ge_{1-x}Sn_xTe$ thin film grown on BaF_2 (111) substrates with different compositions x_{Ge} (shown: 0.30 and 0.60), evidencing the transition from the cubic (left) to the rhombohedral phase (right) with increasing Ge content. (*right*) Temperature dependent ARPES $E(k)$ spectra of a (111) oriented $Pb_{0.54}Sn_{0.46}Te$ thin film measured near the Γ point (shown: 300 K and 54 K).

ordered state as below T_C). A proper understanding of the phase transition is crucial for topological phase diagram of $Pb_{1-x}Sn_xTe$ and $Ge_{1-x}Sn_xTe$ since it determines if above T_C the lattice becomes fully symmetric (which favors the TCI phase) or retains some of the broken symmetry (which favors the FERS or trivial phase).

2 Objectives

The experiments described in this proposal are a crucial component in a wider research project aimed to establish a comprehensive understanding of the model class of IV-VI topological crystalline insulators. The project consists of determining the topological phase diagram of $Pb_{1-x}Sn_xTe$ and $Ge_{1-x}Sn_xTe$ epitaxial thin films (grown by molecular beam epitaxy on BaF_2 substrates), with particular emphasis on the underlying role of local structure [as illustrated in 2 (b)].

The specific goal of the experiments proposed here, based on hyperfine interaction (HFI) techniques, is to measure the sublattice displacement in the cubic and rhombohedral phases as well as through the phase transition (which includes determining if the transition is of displacive or order-disorder nature). The required complementary studies are currently underway, most notably: determining the rhombohedral distortion angle α using synchrotron radiatin X-ray diffraction (SR-XRD, e.g. Fig. 3); determining the topological state with angle-resolved photoemission spectroscopy (ARPES, e.g. Fig. 3).

Fulfilling this general goal (drawing the topological phase diagram) will allow us to answer specific questions which are (individually) crucial for the understanding of topological crystalline insulators, for example: Is it possible to design the *ideal* FERS (i.e. can the Rashba splitting in FERS be tuned independently of the band inversion)? Can different topological states such as TCI and FERS coexist (i.e. under finely tuned band inversion and local structure conditions)? Is the TCI phase resistant to weak symmetry breaking (i.e. how large must the rhombohedral distortion be to destroy the TCI behavior)? For

example, our ARPES data (Fig. 3) has shown that $Pb_{0.54}Sn_{0.46}Te$ is in a trivial state at 110 K, while at 54 K the band gap is closed; we believe that this is due to thermally activated local rhombohedral distortions and *not* (or at least not only) an effect of temperature on the band inversion as generally assumed (cf. e.g. Ref. [17] and references therein).

3 Methodology

Limitations of more conventional techniques. X-ray diffraction, although ideal to measure the lattice constant and α, is not suitable to measure the sublattice displacement.[15;16] The *standard* technique to probe such local distortions is extended X-ray absorption fine structure (EXAFS).[15;16] However, high precision in Δr (ideally ~ 0.01 Å in the present case) can only be achieved in the near-bulk regime, by measuring *transmission* EXAFS of thick films (optimal thickness of tens of micron for measurements on the Sn and Te K-edges, for example) which are deposited on low-Z substrates (to minimize absorption on the substrate).[15;16] High-quality epitaxial thin films (typically grown on BaF_2, thus precluding *transmission* EXAFS) require measurements in *fluorescence* mode, and the overall lower intensities impose strong limitations on the achievable precision in Δr. This is illustrated in Fig. 4: (a) shows a high-quality EXAFS spectrum of a SnTe thick film (10 micron) measured at 5 K in a state of the art EXAFS beam line; (b) plots the precision in Δr obtained from fitting the data in (a) as a function of the upper k limit used in the fit, showing that a precision in Δr of ~ 0.01 Å would require EXAFS measurements up to at least $k_{\max} \approx 14$ Å^{-1}. However, the lower intensity associated with thin films (hundreds of nm or less), together with the strong decrease in the EXAFS oscillation amplitude with increasing temperature (up to hundreds of K),[16] makes it extremely challenging to even reach a $k_{\max}$ of 13 Å^{-1}, therefore limiting the precision of EXAFS in the present context.

Using hyperfine interaction techniques. We propose to determine the sublattice displacement by measuring the nuclear quadrupole splitting (QS) of selected eMS and PAC isotopes. The QS is given by the product of the nuclear quadrupole moment (Q), a property of the nucleus, and the local electric field gradient (EFG) in the neighborhood of the nucleus. Since the EFG is determined primarily by the electrons involved in the bonding with the nearest neighbors, the QS is extremely sensitive to subtle local distortions, as the rhombohedral distortion described above.
Figure 4 (c,d) shows a test measurement on ^{119}In/^{119}Sn eMS on PbTe (implanted with ^{119}In). These measurements strongly support the feasibility of the experiments proposed here in a two-fold manner. First, the detrimental effects of ion implantation (eventual damage/implantation-related components) are minimal and do not disturb the study of the component of interest (i.e. probe atom located on the Pb/sn/Ge site), showing that this class of materials is very well suited for the measurements that we propose. Second, and even more importantly, they show that even small temperature variations of the smallest QS values can be resolved: note that (1) PbTe is always in the cubic phase and has the smallest Δr values of the compounds in question, and (2) ^{119}Sn has the smallest Q of the isotopes that we propose to use (cf. below). Still, we are able to measure a

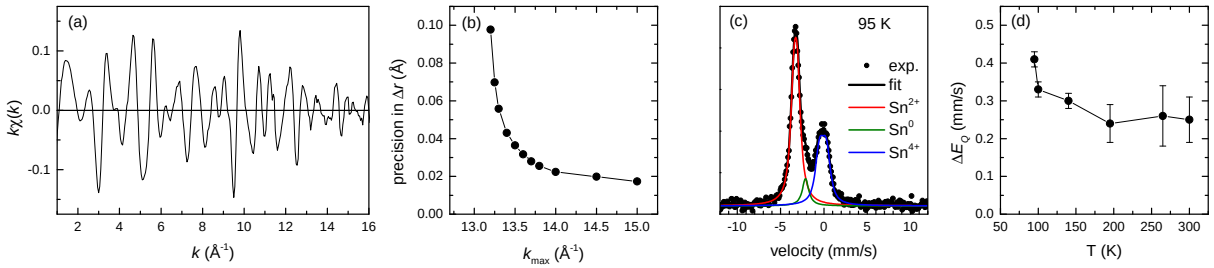

Figure 4: (a) Sn-edge EXAFS spectrum (in fluorescence) of a SnTe thick film (10 micron) measured at 5 K at the EXAFS beam line of the Australian Synchrotron. (b) Precision in Δr as a function of $k_{\max}$ used in the fit of the data in (a). (c) ^{119}Sn:PbTe eMS spectrum from ^{119}In implanted and measured at 95 K. Three components are identified: Sn^{2+} (in Pb sites), i.e. the component of interest in this study; a small Sn^{4+} component from a surface oxide layer (will be minimized in future studies by using a thin capping layer); an almost vanishing Sn^0 which can be attributed to probes located in disordered regions (likely implantation-related). (d) Quadrupole splitting ΔE_Q of the Sn^{2+} (Pb-substitutional) component as a function of implantation/measurement temperature. A transition can be observed around the lowest measured temperature (95 K), indicating a similar behavior for Sn in PbTe (as an impurity) and in SnTe (as a constituent, where $T_C \approx 100$ K).

decrease in QS (ΔE_Q) of about 0.3 mm/s (with increasing temperature) with a precision of 0.02 mm/s i.e. better than 10% (at low temperature; the poorer precision at high temperature can easily be improved by increasing statistics). Since in this case we expect a change in Δr smaller than 0.1 Å (the value for SnTe), this corresponds to a precision better than 0.01 Å for measurements with ^{119}Sn, i.e. significantly better than what is achievable with EXAFS in thin films (in fact, better than EXAFS in general - cf. Fig. 4 b and e.g. Refs. [15;16]). For the other isotopes, with larger Q, we expect an even better precision. We note that the values quoted in this paragraph are only illustrative considerations of the expected precision. The *absolute* value of the sublattice displacement Δr will be *quantitatively* determined by comparing the experimental QS to theoretical values calculated with *ab initio* density functional theory for a varying Δr (using as input the lattice constant and α determined experimentally with SR-XRD). These *ab initio* calculations are currently underway.

These preliminary measurements also illustrate the relevance and importance of the experiments proposed here. Note that the observed decrease in QS (i.e. decrease in Δr for Sn) with increasing temperature suggests that Sn in PbTe has an opposite behavior to that of Pb in PbTe and Sn in SnTe (for which Δr has been reported to increase with temperature[14;16]). The comprehensive study proposed here may therefore show, for example, that the transition of $Pb_{1-x}Sn_xTe$ and related TCIs into a trivial state at higher temperatures (cf. Fig. 3) is, at least partly, due to a temperature-dependent distortion, and *not* simply an effect of temperature on the band inversion as generally believed (cf. e.g. [17] and references therein).

Isotopes and techniques.

Lead (Pb) - PAC. We propose to apply ^{204}Pb PAC (γ-γ) by directly implanting the isomeric ^{204m}Pb state ($t_{1/2}$ = 67 min), from RILIS source.[18] Thanks to its large Q (0.44 b) and the relatively long half-life (256 ns) of the 375 keV intermediate state, ^{204m}Pb is an exceptional probe in this context,[19] with an expected precision in QS better than 10%. Furthermore, its high anisotropy parameter A_{22} (0.25)[20] makes it particularly sensitive to deviations from axial symmetry.[19]

Tin (Sn) - eMS. We propose to use ^{119}Sn eMS, from the decay of implanted ^{119}In ($t_{1/2}$ = 2.4 min). ^{119}In/^{119}Sn eMS has been extensively used in the past (Ref. [21] and references therein). The eMS collaboration resumed the use of this isotope in recent years,[22;23] and the recent development of In RILIS beams have allowed for a 20-fold increase in ^{119}In yields and therefore in measuring speed (^{119}In RILIS run in May/June 2015). The relatively low Q value of the 24 keV Mössbauer state (0.094 b) results, in this case, in a broadened single line rather than a well resolved doublet (Fig. 4 c), but with careful calibration the intrinsic QS values can be determined (d).

In parallel, for selected samples and temperatures, we also propose to carry out eMS measurements by directly implanting ^{119m}Sn ($t_{1/2}$ = 293 d), from RILIS source.[24] Due to the longer half-life (293 d *versus* 2.4 min), it is possible to perform additional measurements offline, including post-implantation annealing and measurements at lower or higher temperatures than those achievable with online eMS. Also, by implanting directly Sn, In-related defects (and recoil) is avoided in such measurements. We note that we will only perform such measurements in selected samples and temperatures (i.e. less extensive than with ^{119}In/^{119}Sn eMS), since the longer half-life implies more time-consuming measurements.

Germanium (Ge) - PAC. We propose to apply ^{73}As/^{73}Ge PAC (γ-e$^-$),[25] by implanting ^{73}As ($t_{1/2}$ = 80 d) from Hot Plasma source, (or RILIS if it becomes available in the meantime). Due to the large Q (0.70 b) and relatively long half-life (2.92 μs) of the 13 keV intermediate state, ^{73}Ge is the most sensitive QS probe from the three proposed here,[25] with an expected precision better than 1%.

Implantation and measurement strategy. The short-lived isotope ^{119}In ($t_{1/2}$ = 2.4 min) will be implanted and measured on-line at GLM (current eMS setup). The long-lived isotopes - ^{204m}Pb ($t_{1/2}$ = 67 min), ^{119m}Sn ($t_{1/2}$ = 293 d), and ^{73}As ($t_{1/2}$ = 80 d) - will be implanted at GLM and measured in the off-line SSP laboratory, after optimal thermal annealing (annealing conditions will be determined with an initial set of samples). We note, however, that our preliminary tests on PbTe, the most radiation-sensitive of the compounds in question, showed no significant detrimental effects related to implantation-induced disorder (cf. above). Required fluence and associated activities are listed in Fig. 5.

Note on the need for radioactive HFI techniques *versus* conventional Mössbuaer spectroscopy. We also carried out feasibility tests with *conventional* ^{119}Sn

beam	$t_{1/2}$	N atoms	fluence (cm^{-2})	Bq	µCi
^{204m}Pb	67 min	2×10^{10}	1×10^{11}	3×10^{6}	90
^{119}In	2.4 min	2×10^{12}	6×10^{12}	1×10^{9} *	27000 *
^{119m}Sn	293 d	1×10^{12}	5×10^{12}	3×10^{4}	0.7
^{73}As	80 d	1×10^{12}	5×10^{12}	1×10^{5}	3

* online measurements (max 20 µSv/h in the GLM area, shielded from users)

Figure 5: Required fluence (in atoms per cm^2) and associated activity (in Bq and μCi) for the requested beams.

MS on a SnTe thin film (i.e. without implantation of radioactive probes). A spectrum with the necessary statistics (comparable to that in Fig. 4 c) requires about 1 month of continuous measurement. Considering that each sample will be measured at several temperatures, and down to Sn concentrations in the few % range, the experiments proposed here would required several years of *conventional* ^{119}Sn MS. For Pb and Ge, there are no suitable stable MS isotopes.

Summary of requested shifts:
Considering the different compositions to be studied as a function of temperature (PbTe, SnTe, GeTe, $Pb_{1-x}Sn_xTe$ and $Ge_{1-x}Sn_xTe$ with 9 values of x: 0.1 - 0.9 in 0.1 steps), we estimate the following number of required shifts:
5 shifts of ^{204m}Pb (UC; LIS) for: (2+9) compositions × 10 temperatures = 110 ^{204m}Pb PAC spectra;
5 shifts of ^{119}In (UC; LIS) for: (3+9+9) compositions × 10 temperatures = 210 ^{119}In/^{119}Sn eMS spectra;
2 shifts of ^{119m}Sn (UC; LIS) for: 5 selected compositions × 5 selected temperatures = 25 ^{119m}Sn eMS spectra;
3 shifts of ^{73}As (YO/ZrO; Hot Plasma or LIS) for: (2+9) compositions × 10 temperatures = 110 ^{73}As/^{73}Ge PAC spectra.

References

[1] E. Plekhanov, P. Barone, D. Di Sante, and S. Picozzi, Physical Review B **90**, 161108 (2014).
[2] T. H. Hsieh *et al.*, Nature Communications **3**, 982 (2012).
[3] M. Serbyn and L. Fu, Physical Review B **90**, 035402 (2014).
[4] J. Liu *et al.*, Nature Materials **13**, 178 (2014).
[5] C. Yan *et al.*, Physical Review Letters **112**, 186801 (2014).
[6] Y. Tanaka *et al.*, Nature Physics **8**, 800 (2012).
[7] Y. Tanaka *et al.*, Physical Review B **88**, 235126 (2013).
[8] S.-Y. Xu *et al.*, Nature Communications **3**, 1192 (2012).
[9] K. Ishizaka *et al.*, Nature Materials **10**, 521 (2011).

[10] G. Landolt *et al.*, Physical Review Letters **109**, 116403 (2012).
[11] A. Crepaldi *et al.*, Physical Review Letters **109**, 096803 (2012).
[12] A. Picozzi, Frontiers in Physics **2**, 10 (2014).
[13] D. Di Sante, P. Barone, R. Bertacco, and S. Picozzi, Advanced Materials **25**, 509 (2013).
[14] E. S. Božin *et al.*, Science **330**, 1660 (2010).
[15] P. Fons *et al.*, Physical Review B **82**, 155209 (2010).
[16] K. Mitrofanov *et al.*, Physical Review B **90**, 134101 (2014).
[17] P. Dziawa *et al.*, Nature Materials **11**, 1023 (2012).
[18] J. Vibenholt *et al.*, Inorganic Chemistry **51**, 1992 (2012).
[19] S. Friedemann, F. Heinrich, H. Haas, and W. Tröger, Hyperfine Interactions **159**, 313 (2004).
[20] N. J. Stone, Atomic Data and Nuclear Data Tables **90**, 75 (2005).
[21] G. Weyer, S. Damgaard, J. Petersen, and J. Heinemeier, Nucl. Instr. Meth. Phys. Res. B **199**, 441 (1982).
[22] H. P. Gunnlaugsson *et al.*, ISOLDE experiment IS-501, **INTC-P-275**, http://cds.cern.ch/record/1232047 .
[23] H. Masenda *et al.*, Hyperfine Interactions **208**, 651 (2013).
[24] U. Köster *et al.*, Nucl. Instr. Meth. Phys. Res. B **266**, 4229 (2008).
[25] J. Correia *et al.*, Hyperfine Interactions **80**, 1321 (1993).

Appendix

DESCRIPTION OF THE PROPOSED EXPERIMENT

The experimental setup comprises: *(name the fixed-ISOLDE installations, as well as flexible elements of the experiment)*

Part of the	Availability	Design and manufacturing
SSP-GLM chamber	☒ Existing	☒ To be used without any modification
On-line eMS setup (@GLM)	☒ Existing	☒ To be used without any modification ☐ To be modified
Off-line eMS setup	☒ Existing	☒ To be used without any modification ☐ To be modified
Off-line PAC setups	☒ Existing	☒ To be used without any modification ☐ To be modified
Annealing furnace @ off-line SSP lab	☒ Existing	☒ To be used without any modification ☐ To be modified

HAZARDS GENERATED BY THE EXPERIMENT

(if using fixed installation) Hazards named in the document relevant for the fixed [COLLAPS, CRIS, ISOLTRAP, MINIBALL + only CD, MINIBALL + T-REX, NICOLE, SSP-GLM chamber, SSP-GHM chamber, or WITCH] installation.

Additional hazards:

Hazards			
	SSP-GLM chamber	On-line eMS setup (@GLM)	Off-line setups @ off-line SSP lab
Thermodynamic and fluidic			
Pressure	Low pressure only	Low pressure only	Low pressure only
Vacuum	10^{-6} mbar during collection	$<10^{-6}$ mbar during collection/measurement	$<10^{-6}$ mbar during measurement or annealing
Temperature	Room temperature	<50°C (outside of setup)	70 K to 1200 K during measurement or annealing
Heat transfer			
Thermal properties of materials			
Cryogenic fluid		N_2, 1 Bar, 3 l/h	N_2, 1 Bar, few liters used during off-line eMS and PAC measurements (in appropriate dewar).
Electrical and electromagnetic			
Electricity			
Static electricity			
Magnetic field			

Batteries			
Capacitors			
Ionizing radiation			
Target material	SnTe, GeTe,PbTe	SnTe, GeTe,PbTe	
Beam particle type (e, p, ions, etc)	ions	ions	
Beam intensity	$<10^9$ s^{-1}	$<10^9$ s^{-1}	
Beam energy	50-60 keV	50-60 keV	
Cooling liquids			Water cooled by chillers with a coolant fluid in closed cycle circuit
Gases			
Calibration sources:			
• Open source			
• Sealed source			
• Isotope			
• Activity			
Use of activated material:			
• Description	☒ Removed from chamber, transported to off-line SSP lab (B.508) in standard Pb shielding.	☒ Sample holders kept in the GLM area at least one hour after implantation; samples stored behind lid and checked for radioactivity afterwards (radioactivity has never been detected day after implantations). The samples are then stored in the designated safes in B.508.	☒ Transported from SSP-GLM chamber to off-line SSP lab (B.508) in standard Pb shielding. Annealed for 10-30 min at temperatures up to 1200 K in tube furnace. Before and after measurement, the active samples are stored in the designated safes in B.508.
• Dose rate on contact and in 10 cm distance	^{204m}Pb: 300 µSv/h @ 10 cm ^{119m}Sn: 3 µSv/h @ 10 cm ^{73}As: 9 µSv/h @ 10 cm	<20 µSv/h inside the GLM area, shielded from users (values from 2015 run).	^{204m}Pb: 300 µSv/h @ 10 cm ^{119m}Sn: 3 µSv/h @ 10 cm ^{73}As: 9 µSv/h @ 10 cm
• Isotope	^{204m}Pb, ^{119m}Sn, ^{73}As	^{119}In	^{204m}Pb, ^{119m}Sn, ^{73}As
• Activity	^{204m}Pb: 90 µCi (3×10^6 Bq) ^{119m}Sn: 0.7 µCi (3×10^4 Bq) ^{73}As: 3 µCi (1×10^5 Bq)	~27 mCi (inside the chamber) (~1 MBq)	^{204m}Pb: 90 µCi (3×10^6 Bq) ^{119m}Sn: 0.7 µCi (3×10^4 Bq) ^{73}As: 3 µCi (1×10^5 Bq)
Non-ionizing radiation			
Laser			
UV light			
Microwaves (300MHz-30 GHz)			
Radiofrequency (1-300MHz)			
Chemical			
Toxic			
Harmful			
CMR (carcinogens, mutagens and substances toxic to reproduction)			
Corrosive			
Irritant			
Flammable			
Oxidizing			
Explosiveness			
Asphyxiant			
Dangerous for the environment			

Mechanical			
Physical impact or mechanical energy (moving parts)			
Mechanical properties (Sharp, rough, slippery)			
Vibration			
Vehicles and Means of Transport			
Noise			
Frequency			
Intensity			
Physical			
Confined spaces			
High workplaces			
Access to high workplaces			
Obstructions in passageways			
Manual handling			
Poor ergonomics			

0.1 Hazard identification

Protocols will be developed/adapted according to beam time (cf. e.g. edms number: 1569671 v.1).

^{204m}Pb beams may exhibit isobaric ^{204}Fr contamination which, as an alpha emitter, requires follow up by RP. The protocol will be adapted accordingly.

Hazard information regarding the target materials:

BaF_2 (10×10×0.5 mm^2 crystals/susbtrates)

http://www.prochemonline.com/upload/MSDS/1189.BariumFluoride.pdf

SnTe (500 nm thin films)

http://www.prochemonline.com/upload/MSDS/3677.Tin(II)Telluride.pdf

PbTe (500 nm thin films)

http://www.prochemonline.com/upload/MSDS/2296.Lead(II)Telluride.pdf

GeTe (500 nm thin films)

http://www.prochemonline.com/upload/MSDS/1931.Germanium(II)Telluride.pdf

3.2 Average electrical power requirements (excluding fixed ISOLDE-installation mentioned above): *(make a rough estimate of the total power consumption of the additional equipment used in the experiment)*